

## Systematics of momentum distributions from reactions with relativistic ions

D. J. Morrissey

*Gesellschaft für Schwerionenforschung, D-6100 Darmstadt, Federal Republic of Germany  
and Department of Chemistry, Michigan State University, East Lansing, Michigan 48824*

(Received 26 July 1988)

The momentum distributions of projectile and target residues from spallation reactions induced by relativistic projectiles already in the literature are transformed into consistent quantities and compared. The momentum imparted to the residual nucleus is presented in terms of a longitudinal velocity,  $\langle\beta_{\parallel}\rangle$ , and a root-mean-squared momentum,  $P_{\text{rms}}$ . These parameters from all spallation products from many disparate systems display the same systematic dependence on observed mass loss. The rms momentum is shown to depend on the square root of the observed mass loss due to momentum conservation in either of three competing processes with no dependence on the initial reaction. The longitudinal momentum is shown to depend on the observed mass loss and therefore on the excitation energy with only a kinematical factor from the entrance channel. Thus, the longitudinal momenta depend on the velocity but not the mass of the reaction partner.

### I. INTRODUCTION

Studies of the remnants of the target and the projectile from relativistic projectile-induced reactions have followed courses as separate as their laboratory velocities. This was due, in large part, to the very different techniques needed to measure the cross sections and momenta of reaction products nearly at rest and those moving with nearly the speed of light. Measurements of the properties of target residues have been made with radiochemical techniques developed for studying relativistic proton-induced reactions whereas projectile fragments have been measured directly in spectrometers.<sup>1-3</sup>

The angle-integrated cross sections for target and projectile fragments have been compared to model calculations on an equal basis for some time. On the other hand, measurements of the momentum distributions of target and projectile residues have been compared neither to the same models nor to each other. This is partly due to the fact that the typical momentum of a target residue is very small and has been directly measured after the residue fissions<sup>4,5</sup> and partly because the momenta deduced from indirect measurements of residue recoil distributions have been presented in so-called convenient units. This has led to separate treatment in review articles of the momentum distributions of target residues and projectile residues.<sup>1-3</sup> Such different treatment is unfortunate because the formation of target and projectile residues must be governed by the same physics, albeit in very different rest frames. Such arbitrary differences between measurements of projectile and target fragmentation products have become moot recently by the acceleration of the heaviest nuclei to relativistic velocities.

The goal of this paper is to correlate directly the data available in the literature on the momenta of projectile and target residues from spallation reactions and identify the physical bases of the empirical distributions. Note that such spallation reactions are limited to peripheral re-

actions in which a residual nucleus with a large fraction of the initial target (or projectile) mass is observed<sup>2</sup> and measurements of target residue recoil distributions from reactions with relativistic protons. However, specific features such as the "enhanced sideways emission" of products from 400 GeV proton-induced reactions<sup>6</sup> or the orbital dispersion observed for heavy-ion-induced reactions with  $T/A \leq 100$  MeV,<sup>7</sup> will not be discussed. Within these limits, all the data will be shown to have the same quantitative dependence on observed mass loss, somewhat contrary to reasonable conclusions drawn from the literature.<sup>8</sup>

The longitudinal momentum distribution of projectile-like residues from carbon-, oxygen-, and argon-induced reactions have been shown to be isotropic in a rest frame moving with nearly the beam velocity.<sup>9,10</sup> (The large widths of the transverse momentum distribution recently obtained for <sup>139</sup>La residues are discussed below.<sup>11</sup>) The targetlike residue momentum distributions, inferred from the recoil-range distributions in a much larger number of reactions, have the corresponding features of essentially isotropic emission in a frame nearly at rest.<sup>1-3</sup> These distributions, as well as the cross sections, are consistent with the assumption that the reaction proceeds through two stages, an initial interaction or fast cascade that is followed by a sequential deexcitation of the precursor nuclei. (The large body of evidence supporting this "two-step" model for peripheral reactions induced by relativistic heavy ions and protons need not be described here.) The momentum distribution thus comes from a convolution of the momentum distribution produced by the primary (or fast) process with that of subsequent sequential decay.

The momentum distributions of all the residues will be presented in terms of the average projection of the velocity distribution on the beam axis,  $\langle\beta_{\parallel}\rangle$ , and an average isotropic recoil momentum,  $P_{\text{rms}}$ . This average recoil momentum is obtained simply:

$$P_{\text{rms}} = \langle P_{\parallel}^2 \rangle^{1/2} \quad (1)$$

from complete momentum distributions such as those published for projectile residues. The average recoil momenta are obtained in a similar manner:

$$P_{\text{rms}} = A_{\text{obs}} \langle V^2 \rangle^{1/2} \quad (2)$$

from the momenta inferred from recoil-range distributions of target residues. The two parameters,  $\langle \beta_{\parallel} \rangle$  and  $P_{\text{rms}}$ , represent the salient information on the momentum distribution that can be reliably extracted from previous measurements of both projectile and target residues. These two parameters were obtained for data in the literature for projectile residues with complete momentum distributions (Refs. 9 and 10) and a large range of target residues from many different reactions.<sup>12-16</sup> Data for residues from reactions with uranium and thorium targets have not been included because the spallation residues cannot be clearly distinguished from fission products without additional assumptions. Data for the longitudinal momentum transfer obtained from fission fragment folding angle distributions was also included.<sup>5</sup> This data spans a broad range of target and projectile mass including two comprehensive studies as a function of bombarding energy.<sup>12,15</sup> However, the reader should recognize that only a fraction of the target residue recoil distributions has been reanalyzed and presented here.

The Gaussian width parameters of the longitudinal momentum distributions of projectile residues are usually interpreted in terms of the relative Fermi momentum of clusters inside the projectile.<sup>17</sup> Goldhaber had previously pointed out that this interpretation is ambiguous because conservation of momentum causes the momentum distribution of a fast breakup process to be the same as that from a single statistical emission of a cluster.<sup>18,19</sup> Friedman has shown that a model based on the separation energies of fragments from the projectile leads to the same functional form and a better representation of the data.<sup>20</sup> On the other hand, the recoil kinetic energy due to the random addition of recoil velocity vectors from any evaporative process, and the "two-step" model in particular, is also known to be approximately linear in mass loss.<sup>21,22,13</sup> In this paper the recoil momenta of projectile and target residues are shown to fall on a common curve. The quantitative agreement of the projectile and target residue data demonstrates the additional ambiguity that the observed distributions could also arise from sequential statistical emission or any combination thereof.

The average longitudinal momentum transfer of all products is shown to be a single function of observed mass loss (thus excitation energy) and projectile velocity but independent of the mass of the reaction partner. The dependence on projectile velocity is contained in a relativistic kinematic factor based on energy and momentum conservation in a simple model of the initial reaction. Such an approach has been used by several authors to describe heavy-ion-induced reactions.<sup>23-25</sup> These ideas have also been applied to proton-induced reactions and lead to the same functional form having differences only in the interpretation of the parameters, see the discussion by Cumming.<sup>26</sup> The smooth dependence of  $\langle \beta_{\parallel} \rangle$  on ra-

pidity ( $Y = \tanh^{-1}\beta$ ) shown by Cumming *et al.*, for a large number of heavy-ion- and proton-induced reactions with copper<sup>15,27</sup> already supports such models. In this paper it is argued that the apparent inconsistencies in the model parameters are a matter of perspective, and a simple functional form describes all of the data. The feature of limiting fragmentation<sup>15</sup> arises naturally in the momentum distributions because the kinematic factor goes to unity as  $\beta \rightarrow 1$ .

The treatment of the projectile residue and the target residue data from the literature are presented separately in the following section. The discussion of the momentum distributions and comparison of the empirically correlated data is contained in Sec. III. The discussion of the isotropic momentum component is presented first and then that of the longitudinal momentum transfer.

## II. DATA ANALYSIS

### A. Projectile residues

The data from the projectile fragmentation study by Greiner *et al.*<sup>9</sup> were reported as the average momentum shift,  $\langle P_{\parallel} \rangle$ , and the Gaussian width,  $\sigma_{\langle P_{\parallel} \rangle}$ , for the momentum distribution projected onto the beam axis. The value of  $\langle \beta_{\parallel} \rangle$  was obtained in a straightforward manner from the momenta with the definition,  $\beta = P/E$ , as,

$$\langle \beta_{\parallel} \rangle = \frac{\langle P_{\parallel} \rangle}{(m_0^2 + \langle P_{\parallel} \rangle^2)^{1/2}} \quad (3)$$

containing the residue rest mass,  $m_0$ , and the measured momentum shift,  $\langle P_{\parallel} \rangle$ . The value of  $P_{\text{rms}}$  is directly related to the measured width parameter, see, e.g., Ref. 23. Recall for a Gaussian distribution in  $R$  centered on the origin that

$$\langle R^2 \rangle = \sigma_x^2 + \sigma_y^2 + \sigma_z^2 = \sigma_{\parallel}^2 + 2\sigma_{\perp}^2. \quad (4)$$

Thus, the recoil momentum distribution, a Gaussian in the moving frame, can be written in terms of the projections parallel and perpendicular to the beam axis as,

$$\langle P_{\text{recoil}}^2 \rangle = \sigma_{\langle P_{\parallel} \rangle}^2 + 2\sigma_{\langle P_{\perp} \rangle}^2. \quad (5)$$

Experimentally  $\sigma_{\langle P_{\parallel} \rangle}$  is equal to  $\sigma_{\langle P_{\perp} \rangle}$  to within 10 percent, and thus,

$$P_{\text{rms}} \equiv (\langle P_{\text{recoil}}^2 \rangle)^{1/2} \approx \sqrt{3}\sigma_{\langle P_{\parallel} \rangle}. \quad (6)$$

The values of  $P_{\text{rms}}$  for <sup>16</sup>O induced reactions, shown in Fig. 1, were calculated with Eq. (6) and the data in Table 1 of Ref. 9. The values of  $\sigma_{\langle P_{\parallel} \rangle}$  for the residues from <sup>40</sup>Ar projectiles were calculated with the best-fit value of  $\langle \sigma_0 \rangle = 94$  MeV/c, see Fig. 1 in Ref. 10.

Special mention should be made of the very recent measurements of residues from the spallation of <sup>139</sup>La projectiles.<sup>11</sup> Angular distributions and thus the momentum component orthogonal to the beam axis,  $\langle P_x \rangle$ , were obtained as a function of nuclear charge but neither the mass nor the total momentum of the residue were mea-

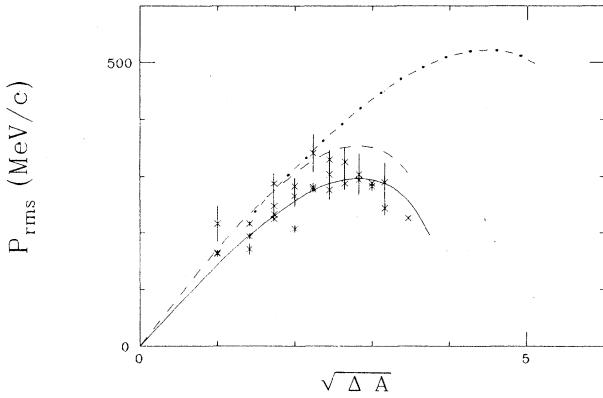


FIG. 1. The recoil momentum,  $P_{\text{rms}}$ , as a function of observed mass loss for projectile residues. The dashed curve was calculated with the Goldhaber model (Ref. 18) and the solid curve is the best fit (Ref. 9). The dotted-dashed curve is the best fit to the results of  $^{40}\text{Ar}$  fragmentation reactions (Ref. 10).

sured. With the assumption that the average charge-to-mass ratio of each isotopic chain is equal to that of the projectile, the observed widths were found to be significantly larger than those observed in the previous studies with low-mass projectiles. The best-fit value of  $\langle\sigma_0\rangle = 169 \text{ MeV}/c$  is nearly twice that of the  $^{40}\text{Ar}$  data. Such an assumption is good for low-mass residues (due to the focusing into the valley of beta stability by sequential decay) but not for heavier residues. The charge-to-mass ratio should be somewhat higher than that of the beta stable projectile due to the preferential emission of neutrons during sequential decay. The effect of a different assumption for the charge-to-mass ratio of the residues is not so clear and these data have not been included in the present study.

### B. Target residues

While the projectile residues from spallation reactions are moving with nearly the beam velocity, the target residues are produced nearly at rest. The small momenta of these residues (that do not fission) have only been measured with radiochemical recoil-range techniques. The raw results obtained from such studies are the fractions of radioisotopes that escape from the target in the forward and backward directions. These fractions are transformed into kinematical quantities using the two-step velocity vector model and standard range-energy tables. Neither a discussion of the historical development of the analysis of target residue recoil distributions nor a description of the two-step vector model analysis and all its possible parameters is within the scope of this paper. Several rather complete discussions of this analysis technique are available in the literature.<sup>28–30,13</sup> The loose coupling of the sequential decay with the initial phase of the reaction (through the induced excitation energy) and the isotropic momentum distribution of sequential decay in the moving frame have been known for some time to be key ingredients for interpreting the momentum distri-

butions of target residues.<sup>31,32</sup> Within the assumptions discussed by the authors,<sup>33</sup> results for the average parallel velocity vector,  $\langle v_{\parallel}\rangle$ , and the average recoil velocity vector,  $\langle V\rangle = (\langle V^2\rangle)^{1/2}$ , appear in the literature in several different forms and with different dimensions. Data from three previous systematic studies of target residue momenta<sup>12,13,15</sup> are used in the present study along with other “typical” results that are meant to be representative of the extensive amount of information in the literature.<sup>34</sup> The additional data are for the reaction of  $^{20}\text{Ne}$  with tantalum<sup>14</sup> and  $^{12}\text{C}$  and protons with silver.<sup>16</sup>

The average longitudinal velocity,  $\langle v_{\parallel}\rangle$ , was reported with the dimensions  $(\text{MeV}/u)^{1/2}$  by Kaufman *et al.*<sup>12</sup> In the other studies, values of  $\langle\beta_{\parallel}\rangle = \langle v_{\parallel}\rangle/c$  were given directly.<sup>15,16</sup> The tabulation made by Winsberg included only the recoil kinetic energies<sup>13</sup> and is used only in the discussion of  $P_{\text{rms}}$ . All the data for the target recoil momenta were converted into the parameter  $P_{\text{rms}}$  with dimensions  $(\text{MeV}/c)$  with nonrelativistic expressions as follows. Kaufman *et al.* reported the mean recoil momenta:

$$P_{\text{rms}} = A_{\text{obs}} \langle V \rangle (\text{MeV } u)^{1/2} \quad (7)$$

with  $A_{\text{obs}}$  being the atomic number of the residue. Loveland *et al.* reported the mean recoil velocity,  $\langle V \rangle$ , in related dimensions  $(\text{MeV}/u)^{1/2}$ . Momenta with dimensions  $\text{MeV}/c$  were obtained from these data with the definition that  $1 \text{ u} = 931.5 \text{ MeV}/c^2$ . Cole and Porile<sup>16</sup> and Winsberg<sup>13</sup> reported the mean recoil kinetic energy,  $\langle T \rangle$ , in  $\text{MeV}$ . The average recoil momenta were calculated in these cases as,

$$P_{\text{rms}} = (2 A_{\text{obs}} \langle T \rangle 931.5)^{1/2} (\text{MeV}/c) . \quad (8)$$

An important conclusion in many of previous studies is that the recoil momenta of spallation products become independent of bombarding energy. Therefore, only the most extensive set of values are presented for the previous studies with several bombarding energies.<sup>12,15</sup> The original data and the converted parameters are given in Tables I–V. The calculated values for  $P_{\text{rms}}$  are shown as a function of the square root of the observed mass loss,  $\Delta A = A_{\text{init}} - A_{\text{obs}}$ , in Figs. 2 and 3. A line is drawn through the data in Fig. 3 with a slope of  $150 \text{ MeV}/c$  representing the semiempirical dependence  $P_{\text{rms}} = 5.1 (\text{MeV}/u)^{1/2} \sqrt{\Delta A}$  discussed below (cf. Fig. 7 in Ref. 35 and Fig. 6 in Ref. 14).

## III. RESULTS AND DISCUSSION

### A. Isotropic component

The dependence of the average recoil momentum on the square root of the mass loss is shown in Figs. 1 and 2. Such a dependence can arise in three different mechanisms simply due to conservation of momentum. Goldhaber has shown that conservation of momentum in sudden breakup of the projectile and in statistical emission of a single fragment leads to a Gaussian momentum distribution.<sup>18</sup> The predicted width of the distribution is related to  $P_{\text{rms}}$  as in Eq. (6):

TABLE I. Data for target recoils from the reaction of GeV protons with  $^{197}\text{Au}$  (Ref. 12). The dimensions of the momenta,  $P_{\text{rms}}$  and  $\langle P'_{\parallel} \rangle$  are MeV/c. The values of  $P_{\text{rms}}$  are given only for 11.5 GeV protons. The values of  $\langle \beta_{\parallel} \rangle$  have been multiplied by 1000.

Nuclide	Proton energy	11.5		1.0		3.0		28		300	
	$\beta\gamma/(\gamma+1)$	$P_{\text{rms}}$	$\langle \beta_{\parallel} \rangle$	$\langle P'_{\parallel} \rangle$	$\langle \beta_{\parallel} \rangle$						
$^{46}\text{Sc}$	1450	1.3	221	3.8	411	4.4	633	0.5	89	0.2	37
$^{48}\text{V}$	1490	0.8	136			4.8	691	0.1	18	0.0	0
$^{54}\text{Mn}$	1480	0.8	136	3.6	389	3.5	504	0.1	18	0.0	0
$^{58}\text{Co}$	1520	0.7	119	4.5	487	3.6	518	0.3	53	0.0	0
$^{59}\text{Fe}$	1640	0.8	136	2.8	303	2.9	417	0.1	18	0.3	55
$^{65}\text{Zn}$	1510	0.7	119	3.1	335	2.9	417	0.1	18	0.0	0
$^{74}\text{As}$	1790	0.9	153	2.6	281	2.7	389	0.4	71	0.6	110
$^{75}\text{Se}$	1520	0.7	119			2.4	345	0.4	71	0.2	37
$^{83}\text{Rb}$	1510	1.0	170	2.4	260	2.6	374	0.7	124	0.5	91
$^{87}\text{Y}$	1550	1.0	170	2.3	249	2.6	374	0.7	124	0.6	110
$^{89}\text{Zr}$	1500	1.0	170	2.4	260	2.7	389	0.7	124	0.6	110
$^{90}\text{Nb}$	1520	1.2	204	2.7	292	2.5	360	0.7	124	0.7	128
$^{96}\text{Tc}$	1510	1.1	187	2.6	281	1.4	201	1.0	178	1.0	183
$^{103}\text{Ru}$	2410	1.4	238	1.6	173	2.8	403				
$^{131}\text{Ba}$	1230	1.6	272	2.9	314	2.6	374				
$^{139}\text{Ce}$	1130	1.5	255	3.1	335	2.6	374	1.4	249	1.2	220
$^{143}\text{Pm}$	1120	1.6	272							1.2	220
$^{145}\text{Eu}$	1120	1.6	272	3.3	357	2.4	345			1.3	238
$^{146}\text{Gd}$	1090	1.6	272	3.3	357	2.4	345	1.4	249	1.2	220
$^{149}\text{Gd}$	1060	1.5	255	3.2	346	2.2	317	1.4	249	1.1	201
$^{167}\text{Tm}$	890	1.1	187	2.5	270	1.5	216				
$^{171}\text{Lu}$	890	1.1	187	2.2	238	1.3	187				
$^{182}\text{Os}$	540	0.7	119								
$^{183}\text{Os}$	520	0.7	119								
$^{185}\text{Os}$	470	0.6	102								
$^{194}\text{Au}$	280	0.3	51								
$^{196}\text{Au}$	180	0.1	17								

TABLE II. Data for the target recoils from the reaction of various projectiles with copper (Ref. 15). The values of  $P_{\text{rms}}$  are given only for the reaction with 28 GeV protons.

Projectile	$T/A$ (GeV)	$^{24}\text{Na}$	$^{28}\text{Mg}$	$^{44m}\text{Sc}$	$^{48}\text{V}$	$^{52}\text{Mn}$	$^{58}\text{Co}$	$\beta\gamma/(\gamma+1)$
		$\langle V \rangle$ (MeV/u $^{1/2}$ )	$P_{\text{rms}}$ (MeV/c)	$\langle \beta_{\parallel} \rangle \times 10^3$				
		0.903	0.828	0.463	0.394	0.345	0.220	
		662	707	623	577	547	390	
$^4\text{He}$	0.18	16.50	15.40	11.80	9.89	8.42	3.93	0.296 83
$^4\text{He}$	0.22	15.00	13.60					0.324 99
$^{12}\text{C}$	0.40	15.60	14.90	8.94	7.21	5.77	2.74	0.420 42
$^1\text{H}$	0.70	8.81	8.72					0.521 08
$^1\text{H}$	0.81	9.11	9.96	6.03	4.95	4.13	2.14	0.548 94
$^4\text{He}$	1.0	10.50	8.42	5.73	4.42	3.64	1.69	0.591 00
$^{12}\text{C}$	1.54	7.47	6.91	4.82	3.80	3.14		0.672 71
$^{12}\text{C}$	2.1	6.65	6.88	4.26	3.47	2.91	1.47	0.727 94
$^1\text{H}$	3.0	7.14	6.82					0.784 22
$^{16}\text{O}$	13.5	4.36	5.14	3.21	2.62	2.23	1.00	0.937 41
$^1\text{H}$	28	5.44	5.41	3.44	2.77	2.41	1.17	0.968 06
$^1\text{H}$	400	5.44	5.41	3.37	2.71	2.36	1.25	0.997 66

TABLE III. Data for the target recoils from the reaction of GeV protons with various targets (Ref. 13), see the original reference.

Nuclide	Target	$T_{\text{proton}}$ (GeV)	$\langle T \rangle$ (MeV)	$P_{\text{rms}}$ (MeV/c)	$\Delta A$ (u)
$^{196}\text{Au}$	$^{197}\text{Au}$	11.5	0.10	190	1
$^{194}\text{Au}$	$^{197}\text{Au}$	11.5	0.25	300	3
$^{185}\text{Os}$	$^{197}\text{Au}$	11.5	0.73	500	12
$^{183}\text{Os}$	$^{197}\text{Au}$	11.5	0.88	550	14
$^{182}\text{Os}$	$^{197}\text{Au}$	11.5	0.96	570	15
$^{58}\text{Co}$	$^{64}\text{Cu}$	28.0	1.3	375	6
$^{24}\text{Na}$	$^{27}\text{Al}$	0.18–0.4	1.85	288	3
$^{149}\text{Tb}$	$^{181}\text{Ta}$	0.45–6.2	2.5	830	32
$^{52}\text{Mn}$	$^{64}\text{Cu}$	28.0	3.0	540	12
$^{22}\text{Na}$	$^{27}\text{Al}$	3–300	2.9	340	5
$^{83}\text{Sr}$	$^{108}\text{Ag}$	2.9	3.2	730	25
$^{48}\text{V}$	$^{64}\text{Cu}$	28.0	3.6	570	16
$^{44}\text{Sc}$	$^{64}\text{Cu}$	28.0	4.6	615	20
$^{24}\text{Na}$	$^{36}\text{Cl}$	2.9	4.3	440	12
$^{18}\text{F}$	$^{27}\text{Al}$	1–11.5	5.9	440	9
$^{62}\text{Cu}$	$^{108}\text{Ag}$	2.9	5.9	810	46
$^{24}\text{Na}$	$^{51}\text{V}$	2.9	6.1	500	27
$^{28}\text{Mg}$	$^{64}\text{Cu}$	3,28.0	10.7	746	36
$^{11}\text{C}$	$^{27}\text{Al}$	1–11.5	8.0	405	16
$^{43}\text{Sc}$	$^{108}\text{Ag}$	2.9	9.4	860	65
$^{24}\text{Na}$	$^{64}\text{Cu}$	3,28.0	9.8	660	40
$^{84}\text{Rb}$	$^{89}\text{Y}$	0.6,10.5	1.2	430	5
$^{83}\text{Rb}$	$^{89}\text{Y}$	0.6,10.5	1.4	465	6
$^{171}\text{Lu}$	$^{197}\text{Au}$	1–11.5	2.4	870	26
$^{167}\text{Tm}$	$^{197}\text{Au}$	1–11.5	2.6	900	30
$^{84}\text{Rb}$	$^{108}\text{Ag}$	0.6–21	3.7	760	24
$^{83}\text{Rb}$	$^{108}\text{Ag}$	0.6–21	4.4	830	25
$^{149}\text{Gd}$	$^{197}\text{Au}$	1–300	4.0	1050	48
$^{149}\text{Tb}$	$^{197}\text{Au}$	1–300	3.8	1030	48
$^{146}\text{Gd}$	$^{197}\text{Au}$	1–300	4.3	1080	51
$^{145}\text{Eu}$	$^{197}\text{Au}$	1–300	4.6	1110	52
$^{143}\text{Pm}$	$^{197}\text{Au}$	11.5,300	4.7	1119	54
$^{149}\text{Tb}$	$^{209}\text{Bi}$	3,6.2	4.9	1170	60
$^{139}\text{Ce}$	$^{197}\text{Au}$	11.5–300	4.8	1110	58

$$P_{\text{rms}} = (3\sigma_{\langle p_{\parallel} \rangle}^2)^{1/2} = \left[ \frac{3p_F^2 A_{\text{obs}} \Delta A}{5(A_{\text{init}} - 1)} \right]^{1/2}, \quad (9)$$

where  $p_F$  is the Fermi momentum and  $A_{\text{init}}$  is the mass number of the initial fragment. Equation (9) with  $p_F = 230$  MeV/c is compared to the data in Figs. 1 and 2. (The characteristic parabolic dependence of  $\sigma_{\langle p_{\parallel} \rangle}$  on  $A_{\text{obs}}$  has been distorted by the square root.) The agreement of this model with projectile residue data is well known.<sup>17</sup> However, the overall quantitative agreement of Eq. (9) with the data for target residues is remarkable. The data for products from reactions with copper and silver follow the curve quite closely and only the recoil momenta of products with large mass losses from heavy targets lie significantly above the curve. The discrepancy increases with target mass.

On the other hand, the isotropic component of the target residue momentum is usually thought to be produced by the random combination of small recoil momenta from sequential evaporation, i.e., a third process.  $P_{\text{rms}}$ , the result of a random walk in recoil momentum space,

TABLE IV. Data for the target recoils from the reaction of 18.5 GeV  $^{12}\text{C}$  and 400 GeV protons with silver (Ref. 16). The values of  $\beta\gamma/(\gamma+1)$  are 0.672 71 and 0.997 66, respectively.

Nuclide	$\langle T \rangle$ (MeV)	$P_{\text{rms}}$ (MeV/c)	$\langle \beta_{\parallel} \rangle$ $\times 10^3$	$\langle P'_{\parallel} \rangle$ (MeV/c)
$^{12}\text{C} + \text{Ag}$				
$^{24}\text{Na}$	22	990	6.7	450
$^{28}\text{Mg}$	22	1070	5.1	345
$^{42}\text{K}$	8.1	800	2.7	180
$^{44}\text{Sc}$	12.1	996	4.6	310
$^{48}\text{Sc}$	24	1470	6.0	410
$^{48}\text{V}$	11.0	993	4.6	310
$^{52}\text{Mn}$	10.2	993	4.8	325
$^1\text{H} + \text{Ag}$				
$^{24}\text{Na}$	18.1	899	3.4	340
$^{28}\text{Mg}$	17.8	962	3.7	370
$^{42}\text{K}$	12.1	974	2.9	290
$^{44}\text{Sc}$	13.2	1040	3.0	300
$^{48}\text{Sc}$	12.1	1040	3.0	300
$^{48}\text{V}$	10.7	979	2.9	290
$^{52}\text{Mn}$	10.1	988	2.9	290

TABLE V. Data for the target recoils from the reaction of 8.0 GeV  $^{20}\text{Ne}$  with tantalum (Ref. 14) similar to Table IV. The value of  $\beta\gamma/(\gamma+1)$  is 0.42042.

Nuclide	$\langle V \rangle$ (MeV/u) $^{1/2}$	$P_{\text{rms}}$ (MeV/c)	$\langle \beta_{\parallel} \rangle$ $\times 10^3$	$\langle P_{\parallel}^{\prime} \rangle$ (MeV/c)
$^{43}\text{K}$	1.02	1340	9.8	695
$^{46}\text{Sc}$	0.960	1345	8.6	610
$^{48}\text{Sc}$	0.998	1460	9.0	640
$^{48}\text{V}$	1.068	1565	9.5	670
$^{54}\text{Mn}$	0.979	1615	8.0	570
$^{65}\text{Zn}$	0.842	1670	5.9	420
$^{74}\text{As}$	0.676	1520	5.2	370
$^{75}\text{Se}$	0.620	1420	4.8	340
$^{83}\text{Rb}$	0.555	1410	5.6	400
$^{84}\text{Rb}$	0.656	1680	5.5	390
$^{87}\text{Y}$	0.510	1350	5.6	400
$^{89}\text{Zr}$	0.524	1430	4.9	350
$^{90}\text{Nb}$	0.486	1330	5.9	420
$^{96}\text{Tc}$	0.503	1475	6.0	425
$^{97}\text{Ru}$	0.448	1330	6.7	475
$^{131}\text{Ba}$	0.276	1100	5.0	350
$^{139}\text{Ce}$	0.245	1040	4.7	330
$^{145}\text{Eu}$	0.217	960	4.3	305
$^{146}\text{Gd}$	0.229	1020	4.2	300
$^{149}\text{Gd}$	0.187	850	3.6	255
$^{167}\text{Tm}$	0.108	550	1.8	130
$^{171}\text{Lu}$	0.090	470	1.4	99

can be quite significant even though the contribution to the rms momentum per step is small (in contrast to assumptions presented in the literature<sup>24,19,11</sup>). Crespo *et al.*<sup>21</sup> have shown that a sequential evaporation chain in which the residue receives an average momentum in each step,  $\langle P_i \rangle$ , leads to the expression

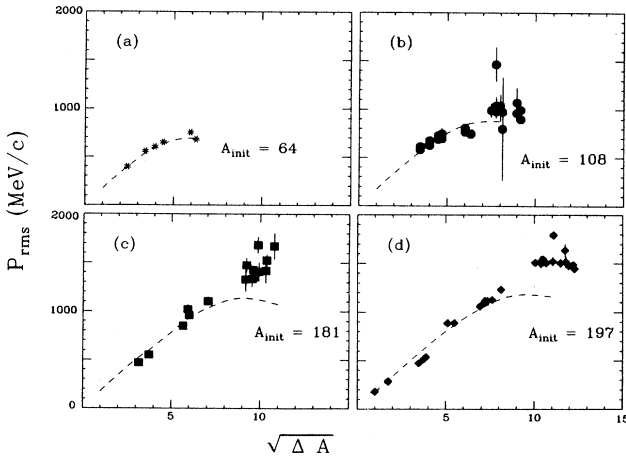


FIG. 2. The recoil momentum,  $P_{\text{rms}}$ , as a function of observed mass loss, similar to Fig. 1, from target residues. The dashed curves were calculated with the Goldhaber model (Ref. 18). The reactions are: (a) 28 GeV protons + Cu (Ref. 15), (b) 18.5 GeV  $^{12}\text{C}$  and 400 GeV protons + Ag (Ref. 16), (c) 8.0 GeV  $^{20}\text{Ne}$  +  $^{181}\text{Ta}$  (Ref. 14), and (d) 3.0 and 11.5 GeV protons +  $^{197}\text{Au}$  (Ref. 12).

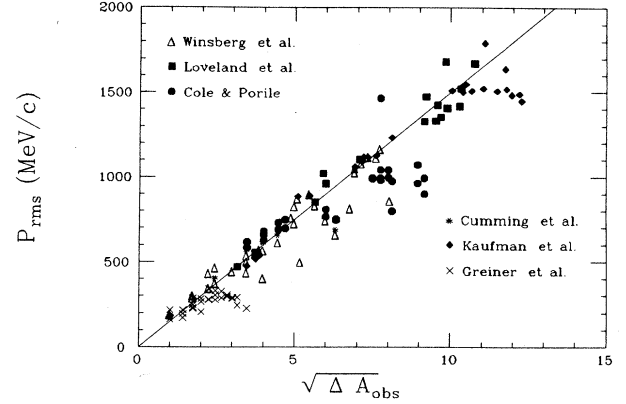


FIG. 3. The combination of the data presented in Figs. 1 and 2. The symbols retain their meaning from Figs. 1 and 2 but the error bars are not shown for clarity. The straight line with a slope of 150 MeV/c/u $^{1/2}$  represents a previous empirical description discussed in the text.

$$P_{\text{rms}} \equiv A_{\text{obs}} \langle V^2 \rangle^{1/2} \approx \langle P_i \rangle \sqrt{\Delta A} = \frac{A_{\text{obs}} \langle p_i \rangle}{A_{\text{avg}}} \sqrt{\Delta A}, \quad (10)$$

where  $A_{\text{avg}}$  is the average mass number of the residue in the chain. The measured values of the recoil kinetic energy imply that the average momentum of the emitted particles,  $\langle p_i \rangle$ , is approximately 175 MeV/c with a small dependence on  $A_{\text{obs}}$ . Notice that Eq. (9) yields approximately the same numerical result for large nuclei in which

$$\frac{A_{\text{obs}}}{A_{\text{init}} - 1} \approx \frac{A_{\text{obs}}}{A_{\text{avg}}}$$

because  $\sqrt{3/5}p_F \approx 175$  MeV/c. Both of these expressions are in good agreement with the smaller slope of the data in Fig. 3 (150 MeV/c) because the multipliers  $A_{\text{obs}}/A_{\text{avg}}$  and  $[A_{\text{obs}}/(A_{\text{init}} - 1)]^{1/2}$  are less than 1 for all the data in the present study.

Starting from Eq. (10), other authors have shown that the average recoil kinetic energy,  $\langle T \rangle$ , of spallation products is proportional to  $\Delta A/A_{\text{obs}}$  with constants of proportionality of 20–40 MeV,<sup>22</sup> 17 MeV,<sup>13</sup> and 20 MeV.<sup>16</sup> This is the same empirical relationship because  $P_{\text{rms}} = (2A_{\text{obs}} \langle T \rangle)^{1/2}$  and the proportionality constant of 20 MeV corresponds to 190 MeV/c.

It should be recognized that the values of  $\langle p_i \rangle$  obtained by fitting Eq. (10) to the data correspond to rather large values of the average total kinetic energy,  $\langle \text{TKE} \rangle$ , of the decay. For example, if the sequential decay chain consisted of only single-nucleon emission then

$$\langle \text{TKE} \rangle \approx \frac{A_{\text{avg}} + 1}{A_{\text{avg}}} \langle p_i \rangle^2 / 2m_n, \quad (11)$$

where  $m_n$  is the nucleon mass. The average residue mass number is usually large compared to 1, so  $\langle \text{TKE} \rangle \approx 12\text{--}16$  MeV/nucleon for values of

$P_{\text{rms}}/\sqrt{\Delta A} = 150\text{--}175 \text{ MeV}/c/u^{1/2}$ . Note also that the excitation energy removed from the nucleus will be larger than the TKE by the separation energy. The typical value for the excitation energy removed per evaluated nucleus in these reactions is thought to be 13 MeV.<sup>36,37</sup> This discrepancy of approximately 50% has been attributed to cluster emission, e.g., in Ref. 13 and also to an inability to separate the "two-steps" of the reaction, e.g., in Ref. 21. With such a large discrepancy it is useful to explore the specific dependence of  $P_{\text{rms}}$  on  $\sqrt{\Delta A}$  in less general statistical deexcitation calculations.

The predicted values of the average recoil momentum for the products of sequential evaporation from excited  $^{197}\text{Au}$  nuclei are shown in Fig. 4. The open circles show the values of  $P_{\text{rms}}$  from the EVA87 version of the DFF code,<sup>38,39</sup> a Monte Carlo cascade evaporation code including complex particle emission but ignoring angular momentum. The code was modified to include calculation of the isotopic and isobaric averages of  $V^2$  and  $P_{\text{rms}}$ . The points in Fig. 4 were obtained by starting the code with a fixed value of excitation energy and then taking the average values of  $P^2$  and  $\Delta A$  for 1000 evaporation chains. The calculated values have the same general features as the data but are always significantly lower. The slope of  $P_{\text{rms}}$  is sensitive to the value of the level density parameter ( $a = A/10$  was used) through its effect on the nuclear temperature and thus on the average kinetic energy of the emitted particles. The difference between the average behavior of the data and the calculations corresponds to an offset of  $\approx 200 \text{ MeV}/c$ .

The result that complex particle emission during the sequential evaporation stage cannot account for the large rms momenta can be clearly demonstrated in a simpler calculation. The solid curves in Fig. 4 result from a schematic Monte Carlo evaporation calculation in which only single nucleons are emitted with the TKE fixed as either 2 or 3 times the nuclear temperature.<sup>40</sup> A Fermi-gas nuclear temperature and an average binding energy of 8 MeV/nucleon were used. The nucleons were emitted

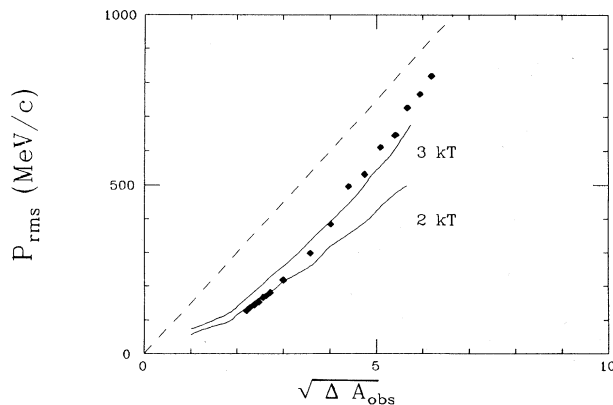


FIG. 4. The calculated recoil momenta of products from  $^{197}\text{Au}$  nuclei are compared to the empirical behavior of the data in Fig. 3, dashed line. The diamonds and solid curves are from Monte Carlo calculations of statistical deexcitation, see the text.

randomly in space, cooling the nucleus, and the chain was terminated when the remaining excitation energy fell below the binding energy. In this simplified calculation each fixed value of the excitation energy leads to a single value of  $\Delta A$ .  $P_{\text{rms}}$  was then calculated from the sum of  $V^2$ 's from many chains. Figure 4 shows that  $\langle \text{TKE} \rangle$  in the EVA87 calculation varies from approximately 2 to 3 kT per particle as the decay chain lengthens. (This is due to increasing charged-particle emission.) The effect of lowering the mass of the initial nucleus all the way to 64 u only leads to an increase of 20–30% in  $P_{\text{rms}}$ , as shown in Fig. 5. Thus, the combination of data from a broad range of initial masses in the present discussion of the average behavior of  $P_{\text{rms}}$  is reasonable.

The effect of cluster-emission in the simpler calculation is shown in Fig. 5. A small increase in  $P_{\text{rms}}$  is observed only for short evaporation chains when the mass of each emitted particle is increased to 2 or 4 u. This result is somewhat contrary to the conventional wisdom that emission of larger mass fragments in an evaporation chain requires larger recoil momenta. While it is true that the recoil from the emission of a single large-mass fragment will be greater than that from emission of a single nucleon,  $P_{\text{rms}}$  is the sum of contributions from the entire evaporation chain. Both calculations show that the emission of a large fragment trades a higher average recoil momentum per step against the removal of a larger amount of excitation energy in that step, and therefore a shorter decay chain. The offset between the average behavior of the data in Fig. 3 and the calculations cannot be attributed to the emission of large fragments, rather it is most likely due to an isotropic momentum component from the initial stage of the collision. The rapid removal of nucleons in the initial stage of the collision, for example, that described by Goldhaber or an intranuclear cascade, would produce such a component.

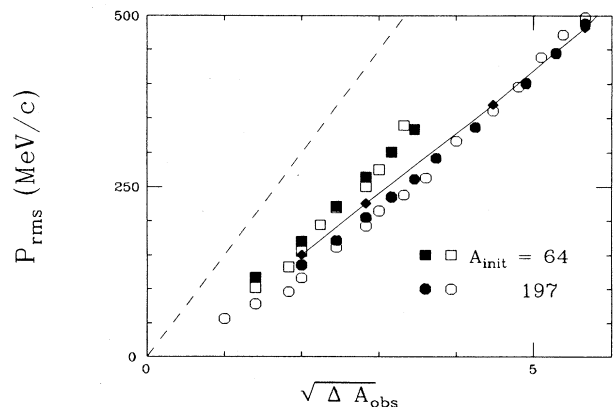


FIG. 5. The recoil momenta of products from statistical deexcitation of nuclei for different initial masses from the schematic model described in the text. A  $\langle \text{TKE} \rangle$  of 2 kT and a binding energy of 8 MeV/nucleon were used with  $\Delta A = 1$  (open symbols), 2 (closed symbols), and 4 ( $A = 197$  only, diamonds). The general behavior of the data in Fig. 3 is indicated by the dashed curve.

In summary, all of the data for the isotropic momentum of projectile and target residues can be described by a simple dependence on the square root of the observed mass loss. This general dependence was shown to be required by momentum conservation. Quantitative comparisons with two statistical evaporation calculations indicate that part of the isotropic momentum is produced in the initial stage of the collision.

### B. Longitudinal momentum

Previous authors have linked the induced momentum in the fast cascade step with (i) the excitation energy of the residue,<sup>41</sup> (ii) the excitation and mass removal,<sup>26</sup> or (iii) a friction due to the removal of bound nucleons.<sup>23,24</sup> Cumming has shown that conservation of energy and momentum in these models leads to the same numerical relation between excitation energy,  $\Delta E_{\text{targ}}$ , and induced momenta,  $q$ .<sup>26</sup> Key assumptions in the derivations are that all the escaping particles are treated as a single object and that  $q$  is small compared to the projectile momentum. Using the parameters of the collective tube model of proton-induced reactions, the relationship between the induced momentum and excitation energy is

$$q_{\text{targ}}c = \frac{\Delta E_{\text{targ}}}{\beta} \left[ 1 + \frac{\Delta m}{\gamma m_p} \right] \quad (12)$$

containing the  $\beta$  and  $\gamma$  of the incident proton and the mass removed from the target,  $\Delta m$ . Using similar arguments Masuda and Uchiyama<sup>25</sup> have shown that essentially the same equation can be obtained for the target residues from heavy-ion-induced reactions:

$$q_{\text{targ}}c = \frac{1}{\beta} \left[ \Delta E_{\text{targ}} + \frac{\Delta E_{\text{proj}}}{\gamma} \right], \quad (13)$$

where the excitation energies of both the projectile and target are included. Both Eqs. (12) and (13) have the same form and can be written

$$q_i c = \frac{\Delta E_i}{\beta} \left[ 1 + \frac{k}{\gamma} \right], \quad (14)$$

where  $k = \Delta m / m_p$  or  $\Delta E_{\text{proj}} / \Delta E_{\text{targ}}$ , respectively. This equation has been fitted to various data in order to extract values for  $\Delta E$  and  $k$ .<sup>13,26,15,5</sup> The typical value for  $k$  is 1 but ranges from 0 to 3 depending on the spallation residue.

Constant values of  $k$  in Eq. (14) are thought to be problematic for heavy-ion-induced reactions. For example, Cumming *et al.*<sup>15</sup> have pointed out that a constant value of  $k = \Delta m / m_{\text{proj}} \approx 1$  is not even consistent with the model.<sup>42</sup> The inconsistency can be avoided if  $m_{\text{proj}}$  is associated with the total mass of the projectile nucleons that *interact* with the target rather than with the total projectile mass. This interpretation follows both the participant-spectator view of heavy-ion collisions<sup>43</sup> and the "loose" binding of nucleons in the projectile and the target used in intranuclear cascade models. Similar arguments that  $k = \Delta E_{\text{proj}} / \Delta E_{\text{targ}} \approx 1$  for different heavy-ion projectiles requires an unlikely accident<sup>5</sup> can be similarly avoided.

One should recognize that the average excitation energy of a residue depends on the average number of removed nucleons (in all models) and the number of removed nucleons should be similar in the participant-spectator models and in intranuclear cascades, at least for peripheral reactions.

Accepting that  $k \approx 1$  in reactions that lead to spallation products, Eqs. (12) and (13) can be written as

$$q_i c \approx \Delta E_i \frac{(\gamma + 1)}{\beta \gamma} \quad (15)$$

with the interpretations: (a) for proton-induced reactions  $\Delta m / m_{\text{proj}} \approx 1$ , (b) for peripheral reactions of heavy ions  $\Delta m_{\text{targ}}$  is approximately equal to the overlapped mass of the projectile, or (c) that  $\Delta E_{\text{proj}} / \Delta E_{\text{targ}} \approx 1$ . Therefore, the momentum transfer should depend only on the induced excitation energy and a kinematic factor. The latter only depends on the kinetic energy per nucleon of the beam and approaches the limiting value of 1 for large values of  $T/A$ . Notice, of course, that  $q_i$  is the momentum of the primary residue and not of the observed product. The excitation energy will be dissipated by the evaporation process. This creates the dispersion about the mean momenta (discussed above), makes  $q_i$  a function of the observed residue mass, and links the two parameters of the momentum distribution.

The most extensive collection of data on the bombarding-energy dependence of the parallel velocity of residues,  $\langle \beta_{\parallel} \rangle$ , is that for a variety of reactions with copper,<sup>15</sup> reproduced in Table II. The momenta of the primary residues can be obtained in the spirit that  $\Delta m / m_{\text{proj}}$  is small by assuming that the mass of the primary residue equals that of the target,  $q \approx m_{\text{targ}} \langle \beta_{\parallel} \rangle$ . The average parallel momentum transfer of the products multiplied by the inverse of the kinematic factor,

$$\langle P'_{\parallel} \rangle \equiv m_{\text{targ}} \langle \beta_{\parallel} \rangle \beta \gamma / (\gamma + 1), \quad (16)$$

is shown as a function of incident kinetic energy per nucleon in Fig. 6. Values of  $\langle \beta_{\parallel} \rangle$  and  $\beta \gamma / (\gamma + 1)$  are given in Table II. Two features of the data are clearly demonstrated in Fig. 6. First, all the data for a given isotope fall on an approximately horizontal line and, second, the height of the line,  $\langle P'_{\parallel} \rangle$ , increases as the observed mass decreases. (The momenta of <sup>24</sup>Na and <sup>28</sup>Mg residues are nearly the same in all cases, the former have been displaced in Fig. 6 for clarity.) The simple kinematic factor removes the bombarding-energy dependence of the parallel momenta from the dependence on observed mass loss. The increase of  $\langle P'_{\parallel} \rangle$  with the mass loss is approximately linear, see below. The linear dependence of a quantity similar to  $\langle P'_{\parallel} \rangle$  on the  $Q$  value has been pointed out for the copper data by Cumming *et al.* in the limit of  $\beta \rightarrow 1$ .<sup>15</sup>

The calculated values of  $\langle P'_{\parallel} \rangle$  [Eq. (16)] for the previous studies of projectile and target residues are combined in Figs. 7 and 8. A range of  $0 < \Delta A \leq 70$  is used in Fig. 7 to emphasize spallation products (the calculated cross sections for spallation products vanish at larger values.<sup>36,37</sup> The momentum transfer increases with the observed mass loss in a common fashion from  $\Delta A = 0$  to

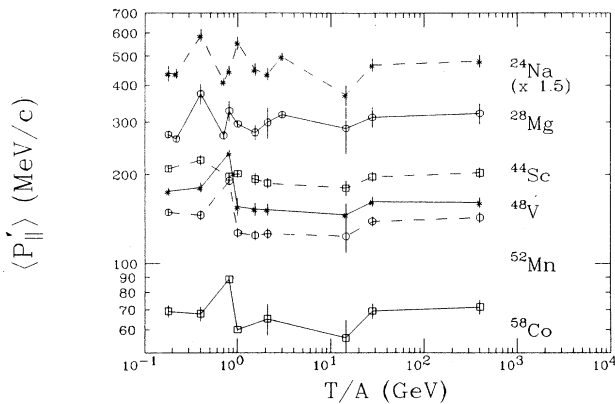


FIG. 6. The average longitudinal momentum transfer for products from various reactions with copper (Ref. 15) is shown as a function of incident kinetic energy per nucleon. The data points for  $^{24}\text{Na}$  fall nearly on top of those for  $^{28}\text{Mg}$  and have been multiplied by 1.5 for clarity. Data points for each isotope are connected by line segments.

50 and then remains approximately constant. The complete range is shown in Fig. 8; values of  $\langle P'_{\parallel} \rangle$  for residues with values of  $\Delta A > 50$  retain some bombarding-energy dependence as these products are produced via a different mechanism. Limiting attention to the spallation residues in Fig. 7, the average longitudinal momenta of the projectile and target residues from a broad range of bombarding energies and masses fall on a common curve. Notice that there is no dependence on the mass of the reaction partner. The rate of change of  $\langle P'_{\parallel} \rangle$  with  $\Delta A$  seen in Fig. 7 is 8 MeV/u.

The mass dependence of the momentum transfer to residues that underwent fission has been measured by

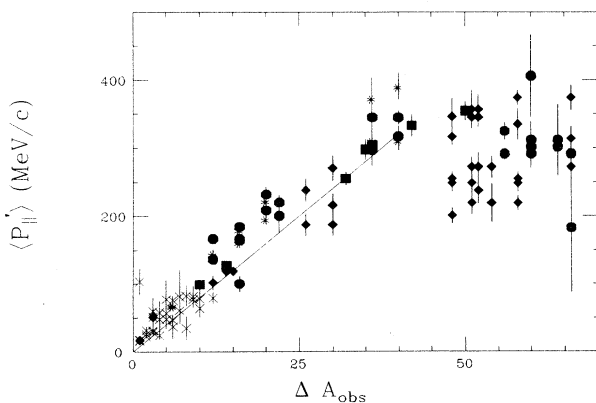


FIG. 7. The average longitudinal momentum transfer as a function of the observed mass loss for the same reactions in Fig. 2. The data for oxygen projectile fragmentation and for 0.4 GeV/nucleon  $^{12}\text{C}$ +copper are also included. The symbols retain their meanings from Figs. 1 and 2. The slope of the solid curve, 8 MeV/u, is taken from Fig. 9.

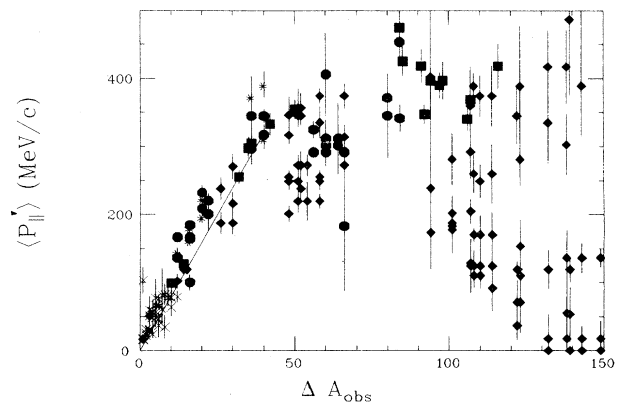


FIG. 8. The average longitudinal momentum transfer as a function of the observed mass loss for the same reactions in Fig. 8 extended to large mass losses.

Kaufman *et al.*<sup>5</sup> for reactions of a variety of relativistic projectiles with gold. These products are complementary to those observed as target residues with recoil techniques. Systematic errors limited the results to the momentum transfer per unit mass loss. The values of  $\langle P'_{\parallel} \rangle / \Delta A$ , shown in Fig. 9, also fall on a horizontal line. The constant value of  $\Delta E / \Delta A \approx 8$  MeV/u is in excellent agreement with all the other data (i.e., the solid line in Figs. 7 and 8). Kaufman *et al.* have argued in their original analysis that the data were consistent with  $k=0$  in Eq. (14), and thus obtained the larger value for the slope of 13 MeV/u.<sup>5</sup> The error bars on the data in Fig. 9 are sufficiently large to encompass both  $k=0$  and 1. The concordance of data in Fig. 7 strongly supports the latter choice.

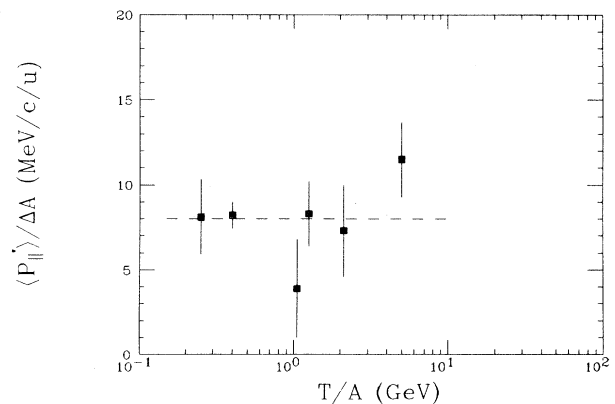


FIG. 9. The average longitudinal momentum transfer per unit mass loss from fission fragment folding angle distributions (Ref. 5) as a function of incident kinetic energy per nucleon. The fission products were observed from the reaction of 5 GeV protons, 1.25 GeV/nucleon  $^4\text{He}$ , 0.25, 0.40, 1.05, and 2.1 GeV/nucleon  $^{20}\text{Ne}$  with  $^{197}\text{Au}$ . A straight line has been drawn through the data at 8 MeV/c/u.

## IV. CONCLUSIONS

The momentum distributions of projectile and target residues from many reactions of relativistic projectiles with a broad range of targets were shown to be quantitatively consistent. The distributions can be described by a longitudinal velocity,  $\langle \beta_{\parallel} \rangle$ , and a recoil momentum,  $P_{\text{rms}}$ . The values of  $P_{\text{rms}}$  depend linearly on the square root of the mass loss as required by momentum conservation. Three different mechanisms for the production of target and projectile residues are shown to give the same quantitative dependence of  $P_{\text{rms}}$  on observed mass. Thus individual contributions cannot be unambiguously identified.

The longitudinal components of the momentum distributions of both the projectile and target residues,  $\langle \beta_{\parallel} \rangle$ , are shown to have the same dependence on beam energy

and total mass loss, but are independent of reaction partner. The values of  $\langle \beta_{\parallel} \rangle$  scaled by a kinematical factor are linear functions of the total mass loss and thus the average excitation energy. Thus, all the data are quantitatively consistent with reaction models that include an initial excitation by rapid removal of bound nucleons from the nucleus and a subsequent sequential decay.

## ACKNOWLEDGMENTS

I would like to thank H. Geisel and K. Sümmerer for many helpful discussions and Z. Fraenkel for providing an up-to-date version of the EVA87 Monte Carlo code. J. B. Cumming provided the detailed data on the target residues from reactions with copper. This work was supported by the Bundesministerium für Forschung und Technologie (Federal Republic of Germany).

- <sup>1</sup>A. S. Goldhaber and H. H. Heckman, *Annu. Rev. Nucl. Part. Sci.* **28**, 161 (1978).
- <sup>2</sup>J. Hüfner, *Phys. Rep.* **125**, 129 (1985).
- <sup>3</sup>E. Friedlander and H. H. Heckman, in *Treatise on Heavy-Ion Reactions*, edited by D. A. Bromley (Plenum, New York, 1987).
- <sup>4</sup>F. Saint Laurent, M. Conjeaud, R. Dayras, S. Harar, H. Oeschler, and C. Volant, *Phys. Lett.* **110B**, 372 (1982); *Nucl. Phys.* **A422**, 307 (1983).
- <sup>5</sup>S. B. Kaufman, M. S. Freedman, D. J. Henderson, E. P. Steinberg, B. D. Wilkins, A. Baden, H. H. Gutbrod, M. R. Maier, J. Péter, H. G. Ritter, H. Stelzer, A. I. Warwick, H. H. Wieman, and F. Weik, *Phys. Rev. C* **26**, 2694 (1982).
- <sup>6</sup>L. P. Remsberg and D. G. Perry, *Phys. Rev. Lett.* **35**, 361 (1975); D. R. Fortney and N. T. Porile, *Phys. Rev. C* **21**, 2511 (1980); J. B. Cumming, P. E. Haustein, and R. W. Steiner, *ibid.* **33**, 926 (1986).
- <sup>7</sup>K. Van Bibber, D. L. Hendrie, D. K. Scott, H. H. Weiman, L. S. Schroeder, J. V. Geaga, S. A. Cessin, R. Treuhaft, Y. J. Grossiod, J. O. Rasmussen, and C. Y. Wong, *Phys. Rev. Lett.* **43**, 840 (1979); J. D. Silk, H. D. Holmgren, D. L. Hendrie, T. J. M. Symons, G. D. Westfall, P. H. Stelson, S. Raman, R. L. Auble, J. R. Wu, and K. Van Bibber, *Phys. Rev. C* **37**, 158 (1988).
- <sup>8</sup>For example, the questions posed at the end of Sec. 4.7 in the recent review by Hüfner, Ref. 2.
- <sup>9</sup>D. E. Greiner, P. J. Lindstrom, H. H. Heckman, Bruce Cork, and F. S. Bieser, *Phys. Rev. Lett.* **35**, 152 (1979).
- <sup>10</sup>Y. P. Viyogi, T. J. M. Symons, P. Doll, D. E. Greiner, H. H. Heckman, D. L. Hendrie, P. J. Lindstrom, J. Mahoney, D. K. Scott, K. Van Bibber, G. D. Westfall, H. Wieman, H. J. Crawford, C. McParland, and C. K. Gelbke, *Phys. Rev. Lett.* **42**, 33 (1979).
- <sup>11</sup>F. P. Brady, W. B. Christi, J. L. Romero, C. E. Tull, B. McEachern, M. L. Webb, J. C. Young, H. J. Crawford, D. E. Greiner, P. J. Lindstrom, and H. Sann, *Phys. Rev. Lett.* **60**, 1699 (1988).
- <sup>12</sup>S. B. Kaufman, E. P. Steinberg, and M. W. Weisfield, *Phys. Rev. C* **18**, 1349 (1978).
- <sup>13</sup>L. Winsberg, *Phys. Rev. C* **22**, 2116 (1980); **22**, 2123 (1980).
- <sup>14</sup>W. Loveland, D. J. Morrissey, K. Aleklett, G. T. Seaborg, S. B. Kaufman, E. P. Steinberg, B. D. Wilkins, J. B. Cumming, P. E. Haustein, and H.-C. Hseuh, *Phys. Rev. C* **23**, 253 (1981).
- <sup>15</sup>J. B. Cumming, P. E. Haustein, and H.-C. Hseuh, *Phys. Rev. C* **24**, 2162 (1981).
- <sup>16</sup>G. D. Cole and N. T. Porile, *Phys. Rev. C* **25**, 244 (1982).
- <sup>17</sup>For example, D. K. Scott, *Nucl. Phys.* **A354**, 375c (1981), and references therein.
- <sup>18</sup>A. S. Goldhaber, *Phys. Lett.* **53B**, 306 (1974).
- <sup>19</sup>G. N. Bertsch, *Phys. Rev. Lett.* **46**, 472 (1981).
- <sup>20</sup>W. A. Friedman, *Phys. Rev. C* **27**, 569 (1983).
- <sup>21</sup>V. P. Crespo, J. B. Cumming, and J. A. Alexander, *Phys. Rev. C* **2**, 1777 (1970).
- <sup>22</sup>J. B. Cumming and K. Bächmann, *Phys. Rev. C* **64**, 1362 (1972).
- <sup>23</sup>A. Abul-Magd, J. Hüfner, and B. Schürmann, *Phys. Lett.* **60B**, 327 (1976).
- <sup>24</sup>A. Abul-Magd and J. Hüfner, *Z. Phys. A* **277**, 379 (1976).
- <sup>25</sup>N. Masuda and F. Uchiyama, *Phys. Rev. C* **15**, 1598 (1977).
- <sup>26</sup>J. B. Cumming, *Phys. Rev. Lett.* **44**, 17 (1980).
- <sup>27</sup>J. B. Cumming, P. E. Haustein, and H.-C. Hseuh, *Phys. Rev. C* **18**, 1372 (1978).
- <sup>28</sup>An early review and discussion is given by J. M. Miller and J. Hudis, *Annu. Rev. Nucl. Sci.* **9**, 159 (1959).
- <sup>29</sup>J. M. Alexander, in *Nuclear Chemistry*, edited by L. Yaffe (Academic, New York, 1968), Vol. I, p. 273; L. Winsberg and J. M. Alexander, *ibid.*, Vol. I, p. 340.
- <sup>30</sup>L. Winsberg, *Nucl. Instrum. Methods* **150**, 465 (1978), and references therein.
- <sup>31</sup>N. Sugarman, M. Campos, and K. Wielgoz, *Phys. Rev.* **101**, 388 (1956).
- <sup>32</sup>A. M. Poskanzer, J. B. Cumming, and R. Wolfgang, *Phys. Rev.* **129**, 374 (1963).
- <sup>33</sup>Important assumptions are that the two steps are sufficiently separated in time that the sequential decay is independent of the initial interaction and that the distributions of the two velocity vectors are narrow with  $\langle v_{\parallel} \rangle \ll \langle V \rangle$ .
- <sup>34</sup>For additional references see Refs. 1–3. Additional evaluation of data in the literature, not presented, is consistent with that presented here except in cases where the contribution to the residue yield of sequential fission cannot be removed.
- <sup>35</sup>S. B. Kaufman, E. P. Steinberg, B. D. Wilkins, and D. J. Hen-

- derson, Phys. Rev. C **22**, 1897 (1980).
- <sup>36</sup>A. Y. Abul-Magd, W. A. Friedman, and J. Hüfner, Phys. Rev. C **34**, 113 (1986).
- <sup>37</sup>A. J. Cole and R. Cherkaoui-Tadili, Phys. Rev. C **36**, 1484 (1987).
- <sup>38</sup>Y. Yariv and Z. Fraenkel, Phys. Rev. C **20**, 2227 (1979); **24**, 488 (1981).
- <sup>39</sup>I. Dostrovsky, Z. Fraenkel, and G. Friedlander, Phys. Rev. **129**, 374 (1963).
- <sup>40</sup>This replaces the kinetic-energy degree of freedom of each step by a fixed value. The most probable neutron kinetic energy is 2 kT; protons will have the additional Coulomb energy of very roughly 2 kT when emitted from a large nucleus. Thus, 3 kT represents a typical kinetic energy for an equal mixture of neutrons and protons emitted from a heavy nucleus.
- <sup>41</sup>L. P. Remsberg, Phys. Rev. **138**, B572 (1965).
- <sup>42</sup>An analysis of the induced momenta for reactions with copper gives  $k = 1$ , see Fig. 4 in Ref. 15. Thus  $\Delta m / m_{\text{proj}} = 1$  implies the impossible result that  $\Delta m = 12$  for near-target residues such as  $^{58}\text{Co}$  from reactions with  $^{12}\text{C}$ .
- <sup>43</sup>J. D. Bowman, W. J. Swiatecki, and C. F. Tsang, Lawrence Berkeley Laboratory Report No. LBL-2908; see also J. Hüfner, K. Schäfer, and B. Schümann, Phys. Rev. C **12**, 188 (1975); J. Gossett, H. H. Gutbrod, W. G. Meyer, A. M. Poskanzer, A. Sandoval, R. Stock, and G. D. Westfall, Phys. Rev. C **16**, 629 (1977).